

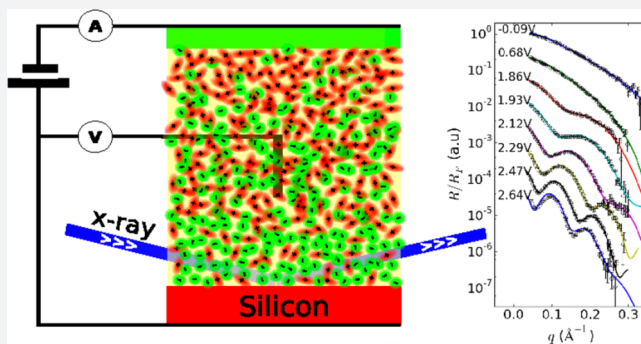
1 Crowding and Anomalous Capacitance at an Electrode–Ionic Liquid 2 Interface Observed Using Operando X-ray Scattering

3 Miaoqi Chu, Mitchell Miller, and Pulak Dutta*

4 Department of Physics & Astronomy, Northwestern University, Evanston, Illinois 60208, United States

5 **S** Supporting Information

6 **ABSTRACT:** Room temperature ionic liquids are widely
7 recognized as novel electrolytes with properties very different
8 from those of aqueous solutions, and thus with many potential
9 applications, but observing how they actually behave at
10 electrolytic interfaces has proved to be challenging. We have
11 studied the voltage-dependent structure of
12 $[\text{TDTHP}]^+[\text{NTF}_2]^-$ near its interface with an electrode,
13 using in situ synchrotron X-ray reflectivity. An anion-rich layer
14 develops at the interface above a threshold voltage of +1.75 V,
15 and the layer thickness increases rapidly with voltage, reaching
16 ~ 6 nm (much larger than the anion dimensions) at +2.64 V.
17 These results provide direct confirmation of the theoretical
18 prediction of “crowding” of ions near the interface. The
19 interfacial layer is not purely anionic but a mixture of up to $\sim 80\%$ anions and the rest cations. The static differential capacitance
20 calculated from X-ray measurements shows an increase at higher voltages, consistent with a recent zero-frequency capacitance
21 measurement but inconsistent with AC capacitance measurements.



22 ■ INTRODUCTION

23 Room temperature ionic liquids (RTILs) are salts with
24 molecular anions and/or molecular cations, which are in the
25 liquid phase at or near room temperature.^{1,2} They are typically
26 nonvolatile, do not require the presence of solvents to be liquid,
27 and have large electrochemical windows. Over the past decade
28 there has been an explosion of interest in ionic liquids, driven
29 both by the synthesis of many different anions and cations³ and
30 by potential applications that range from electrolytes to
31 supercapacitors to electrically controlled lubricants to electro-
32 deposition of metals and alloys.^{4–6}

33 Central to the presumed novelty of RTILs is the idea that the
34 molecules are largely dissociated, i.e., the liquids have very high
35 ionic densities (although this has been disputed^{7–10}). Further,
36 the molecular ions are much larger than typical ions in aqueous
37 solutions, and often have irregular shapes. Thus, there is general
38 agreement that RTILs must behave very differently from
39 aqueous solutions, in particular at interfaces. For example, the
40 Gouy–Chapman–Stern (GCS) picture of the electrolyte near
41 an electrode¹¹ predicts a tightly bound Stern monolayer
42 followed by a diffuse monotonic charge distribution. This
43 picture has been found to be applicable at a variety of dilute
44 electrolytes near electrodes,¹¹ and has been directly confirmed
45 by X-ray standing wave studies.¹² However, the differential
46 capacitance of the RTIL–electrode interface shows anomalous
47 behavior as a function of voltage, frequency, etc.: the curves are
48 bell-shaped or camel-shaped, which are inconsistent with the
49 GCS picture.^{5,7,13} This behavior must originate from the
50 nanoscale structure of RTILs near electrode interfaces, but

what that structure is and how it depends on the applied
51 voltage are poorly understood.

52 As is frequently the case with liquids, a considerable amount
53 of information about interfacial RTILs comes from the
54 predictions of simulations and mean field theories rather than
55 from (relatively difficult) experiments. For example, Kirchner et
56 al.,¹⁴ using molecular dynamics, predict a multilayer structure
57 (alternating anions and cations) at low surface charge, with a
58 transition to a dense counterion monolayer as the electrode
59 surface charge increases. Kornyshev¹³ predicted crowding
60 (formation of a thick counterion layer) using mean field
61 theory. A progression from overscreening (with alternating
62 anion/cation layers) to crowding as a function of ion density,
63 charge, or voltage has been observed in molecular dynamics
64 simulations^{7,15,16} and Landau–Ginsburg theory.^{17,18} Ivaništšev
65 et al.,^{19,20} using molecular dynamics, also predict the formation
66 of an alternating cation–anion layered structure that transitions
67 to a crowded interface layer at higher surface charge. These
68 predicted structures, which are different from those expected in
69 aqueous solutions of ions, may help explain why systems using
70 RTIL electrolytes behave differently from traditional electro-
71 lytes. (It is impractical to provide a comprehensive review of
72 the status of the theory here; see ref 21 for an overview.)
73

74 There are only a few experimental tools that can look at the
75 nanoscale charge distribution normal to an RTIL–solid
76 interface. X-ray and neutron reflectivity are two such tools.

Received: January 18, 2016

77 Neutrons have been used to study RTILs,^{22,23} and have
78 significant advantages in studies of organic molecules that can
79 be selectively deuterated. However, synchrotron X-ray beams
80 have much higher usable flux for studies requiring a low
81 incidence angle at a surface or interface. X-rays are only
82 sensitive to the total electron density and cannot distinguish
83 anions from cations based on their charge. However, the anion
84 and cation will in general have different electron densities, and
85 thus a nonuniform electron density profile at an electrode–
86 RTIL interface means that there is a nonuniform interfacial
87 charge density profile.

88 There have been several previous studies of RTIL structure
89 near solid surfaces^{24–27} where there is no applied voltage and
90 no way to measure the surface charge in situ. In refs 24 and 25,
91 the reflectivity data for an RTIL on insulating (sapphire)
92 substrates, assumed to be charged due to X-ray exposure, were
93 fitted assuming alternating cation/anion layers. However, in ref
94 26 similar layering was reported using uncharged (hydroxy-
95 lated) sapphire. Thus, Uysal et al.²⁸ have correctly noted that
96 the observed layering may have the same origin as that seen
97 even in nonionic molecular liquids.²⁹ Reference 27 reported a
98 dense layer at a presumably uncharged graphene surface, but
99 alternating cation and anion layers at a presumably charged
100 mica surface.

101 There have also been some X-ray studies of RTIL structure
102 using applied voltages at conducting substrates (electrodes).
103 Yamamoto et al.³⁰ used a gold electrode and determined the X-
104 ray reflectivity at one positive and one negative voltage; these
105 differed slightly. Although the reflectivities were monotonic (no
106 interference maxima or minima), the data were fitted using a
107 distorted crystal model (implying layering at the interface).
108 Uysal et al.³¹ used epitaxial graphene on SiC wafers as the
109 electrode, and also reported alternating anion/cation layers in
110 the interfacial RTIL studied at the largest positive and negative
111 voltages used. In a subsequent work, Uysal et al.²⁸ studied the
112 same RTIL at intermediate voltages, and found that the
113 structure was a combination of the two extreme-voltage
114 structures.

115 Experiments using force measurements, the only other
116 applicable technique with comparable spatial resolution normal
117 to the interface, also reach a variety of conclusions. Atomic
118 force microscopy data indicate layered structures near gold³²
119 and pyrolytic graphite³³ electrodes, with the number of layers
120 being a function of applied voltage. However, measurements
121 using a surface force apparatus,⁹ which can be thought of as
122 replacing the AFM tip with an essentially flat mica surface,
123 indicate the presence of an adsorbed ion layer followed by a
124 monotonic diffuse distribution, consistent with the GCS model.

125 Our X-ray reflectivity study departs from previous studies in
126 crucial ways. First, since gold has an extremely high electron
127 density (4660 electrons/nm³, over an order of magnitude
128 greater than typical ionic liquids), the X-ray reflection from
129 gold³⁰ swamps the reflection from RTIL interfacial structures of
130 interest. We used H-terminated silicon substrates instead:
131 silicon has an electron density of ~ 700 electrons/nm³, only
132 about twice that of the typical RTIL. In the Supporting
133 Information we show that a given interfacial structure will lead
134 to visible interference features in the X-ray reflectivity if the
135 substrate is silicon, but not if it is gold. Second, we used an
136 RTIL that has a wide electrochemical window, allowing us to
137 apply higher voltages, as well as a strong electron density
138 contrast between anion and cation. We performed a detailed
139 study as a function of voltage, rather than one or two voltages

as in some previous studies.^{30,31} This allowed us to observe
clear trends in the interfacial structure as a function of the
applied voltage. Our results differ substantially from those
reported in ref 28, but note that the RTILs studied were not
exactly the same (same anion, different cation).

It should be noted that the use of a semiconductor electrode
introduces some complexities¹¹ when the electrolyte is a better
conductor than the electrode. That is not the case here: the
RTIL electrical conductivity (~ 1 – 10 mS/cm) is much lower
than that of the p-type silicon substrates we used (33–1000
mS/cm). Further, all our observations were performed within
the electrochemical window and thus at negligible current
density.

RESULTS AND DISCUSSION

The RTIL studied was trihexyltetradecylphosphonium bis-
(trifluoromethylsulfonyl)imide ([TDTHP]⁺[NTF₂]⁻), see Fig-
ure 1. See Methods for a description of our experimental layout.

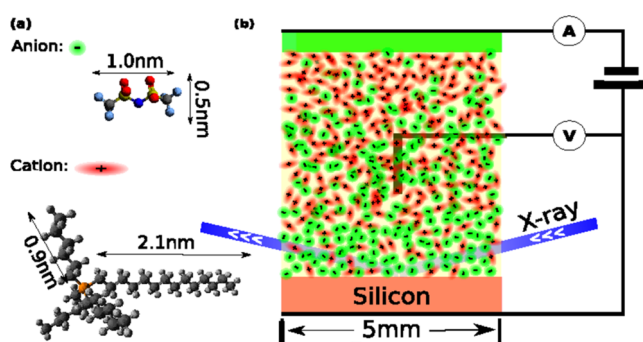


Figure 1. (a) The dimensions and molecular structures of anion and cation used in our experiment. Atoms are represented by colors as follows: red = O, dark blue = N, yellow = F, light blue = S, orange = P, black = C, gray = H. Black and gray spheres are C and H atoms. (b) Schematic diagram of the experiment, showing the grazing incidence X-ray geometry (angle of incidence exaggerated).

Figure 2 shows a cyclic voltammogram obtained using our
experimental setup. The electrochemical window (EW), within
which it is assumed that there is no electrolysis, is typically
defined as the voltage range in which the current is less than
0.1–1.0 mA/cm².³⁴ The ions in our RTIL, [TDTHP]⁺ and

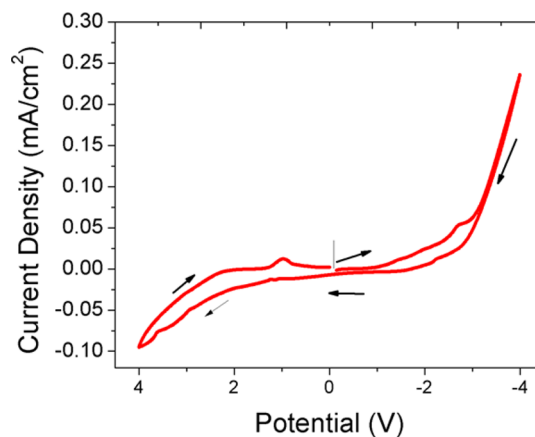


Figure 2. Cyclic voltammogram for [TDTHP]⁺[NTF₂]⁻ measured in our experimental setup, i.e., with Si and Au electrodes. The vertical line and arrows indicate the starting point and scan direction.

162 [NTF₂]⁻, have some of the largest electrochemical-window
 163 potentials among common RTIL anions and cations,^{5,34,35}
 164 -3.64 V and +2.70 V respectively. Figure 2 is consistent with
 165 these numbers.

166 X-ray reflectivity data depend on the electron density profile
 167 normal to the reflecting interface, $\rho_s(z)$, averaged over the
 168 interface plane (i.e., over the x - and y -directions). As previously
 169 noted, X-rays are sensitive to the total electron density,
 170 including all electrons in each atom. In the RTIL studied, there
 171 is a significant difference between the sizes and electron
 172 densities of the anion and cation. The bulk RTIL has electron
 173 density $\rho_{\text{IL}} = 347$ electrons/nm³. The cation is large (0.95 nm³)
 174 and has only slightly lower density than the bulk liquid (289
 175 electrons/nm³), while the anion is small (0.24 nm³) and is
 176 much denser than the bulk (577 electrons/nm³). (See the
 177 Supporting Information for the origin of these numbers.) The
 178 difference in electron density allows us to interpret any
 179 deviations from the bulk RTIL electron density as due to an
 180 imbalance between cations and anions, and thus to calculate the
 181 charge density. Specifically, assuming that the cation (anion)
 182 carries charge of Q ($-Q$), the charge density ρ_c can be
 183 calculated from

$$\rho_c = Q(\rho_s - \rho_{\text{IL}}) \frac{V_a + V_c}{V_a N_c - V_c N_a} \quad (1)$$

184
 185 where ρ_s and ρ_{IL} are the electron density at the interface and
 186 the average electron density of the bulk ionic liquid. V_a (V_c) and
 187 N_a (N_c) are the effective volume of, and number of electrons in,
 188 one anion (cation). Note that this equation does not allow for
 189 compression at the interface (which would change V_a and/or
 190 V_c), and assumes that the ions do not have fractional charge.
 191 These possibilities are discussed later in the paper.

192 The etched silicon (111) surface can undergo surface
 193 reconstruction,³⁶ leading to a relatively rough surface which
 194 causes interfacial reflectivity data to drop rapidly with increasing
 195 q . Flux attenuation during transmission through the bulk RTIL,
 196 and scattering background from bulk IL (which has a broad
 197 peak around 0.41 Å⁻¹), further reduce the highest momentum
 198 transfer in a reflectivity scan q_{max} to 0.30 Å⁻¹, corresponding to
 199 a spatial resolution function of width $\pi/q_{\text{max}} \approx 1$ nm.

200 Figure 3 shows X-ray reflectivity data R divided by the ideal
 201 Fresnel reflectivity R_F , as a function of applied voltage
 202 (measured between the Si substrate and the reference
 203 electrode). At negative voltages (Si electrode at negative
 204 potential relative to the reference electrode), the reflectivity
 205 curves are featureless. We attribute this to the poor density
 206 contrast between the bulk liquid and the cations that are
 207 presumably attracted to the electrode surface. These data are
 208 not shown in this paper. For positive voltages, the reflectivity
 209 curves are featureless at low voltages. Featureless curves can still
 210 be (and often are) fitted with postulated models, but the
 211 conclusions are not robust. However, at higher voltages,
 212 oscillations begin to appear, and the minima shift to lower q as
 213 the applied voltage increases. Such oscillatory features allow
 214 more definitive fits to the data. At each voltage, it takes about
 215 20 min for the reflectivity curve to become stable, i.e., for the
 216 interfacial structure to form. The data are then stable over a
 217 period of at least 40 min, showing that they are not electrolysis
 218 products collecting with time. Our data were also reproducible
 219 in multiple samples.

220 The general procedures for fitting X-ray reflectivity data have
 221 been discussed elsewhere. Here we address the choice of model

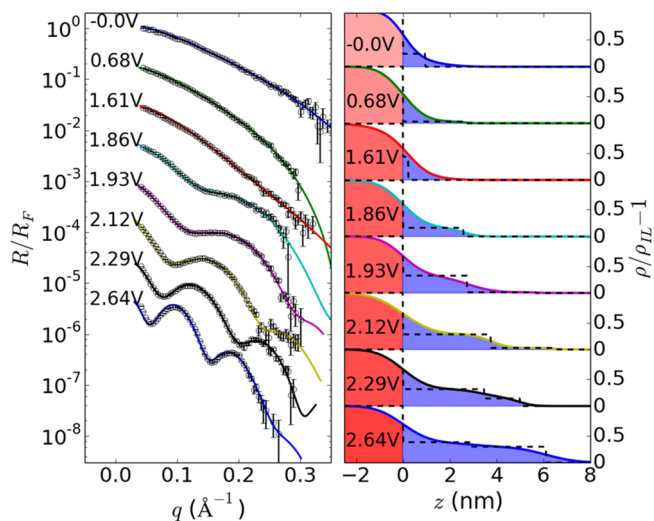


Figure 3. Left: voltage dependent X-ray reflectivity data (open circles) and fits using the slab model discussed in the text (solid lines). The curves are shifted vertically relative to each other for clarity. Right: the voltage-dependent electron density enhancement profiles, $(\rho(z) - \rho_{\text{IL}})/\rho_{\text{IL}}$ where ρ_{IL} is the bulk liquid density, obtained from slab model fits to the data. The dashed lines show the slabs without interface broadening (roughness); the smooth curves show the roughness-broadened profiles. red = Si electrode; blue = anions.

to fit the data. In many previous studies,^{24,30,37} a distorted
 222 crystal model has been used to fit the reflectivity curve. In this
 223 model as applied to an ionic liquid, there are alternating layers
 224 of cations and anions, with each layer having the same charge
 225 but becoming increasingly diffuse (broad) until the structure
 226 becomes that of the bulk liquid. This might happen if there is
 227 overcharging: the first layer of anions carries more charge than
 228 necessary, which requires a subsequent layer of anions, resulting
 229 in charge oscillations decaying into the bulk liquid. When there
 230 are maxima and minima in the reflectivity, a simple slab model
 231 (interfacial steps of variable width, density, and interface
 232 roughness) will also fit the data. 233

We have found that the distorted crystal model will fit our
 234 data only if the Si surface is given a very large roughness (>2
 235 nm), and this indicates that there is a dense interfacial layer that
 236 the distorted crystal model by itself cannot capture (see
 237 Supporting Information for details). The authors of ref 31 have
 238 also found that the distorted crystal model must be
 239 supplemented with an interfacial slab to fit the data from a
 240 similar system. Further, since our data were collected at
 241 multiple voltages and show the reflectivity minimum moving to
 242 smaller q with increasing voltage, the thickness of every layer in
 243 the alternating-layer picture would have to increase continu-
 244 ously with voltage, which is not expected in the distorted crystal
 245 model. We are able to fit our data with interfacial slabs, without
 246 adding alternating anion-cation layers. Of course, a slab model
 247 is also an approximation to reality: it is a “pixelated”
 248 representation of the actual density profile, taking into account
 249 the finite spatial resolution of the reflectivity technique. 250

As shown in Figure 3, the reflectivity curve is featureless at
 251 and below 1.61 V, but develops features (fringes) above that
 252 voltage. We fitted all data using either one or two slabs, but
 253 when there are no features, the fits naturally do not give
 254 significant results. Up to 2.12 V, the data can be fitted using just
 255 one interfacial slab. The data at higher voltages can also be
 256 fitted with one slab, but the fit is slightly improved by using two
 257

258 adjacent slabs. This suggests that the actual electron density
259 profile is rounded such that two “pixels” represent the actual
260 profile better than one uniform-density slab can. However, the
261 basic features of the interfacial region (total thickness, average
262 density) remain essentially the same whether a one-slab or two-
263 slab fit is used.

264 The fitting parameters are tabulated in the Supporting
265 Information. Figure 4 shows the slab thickness (total thickness

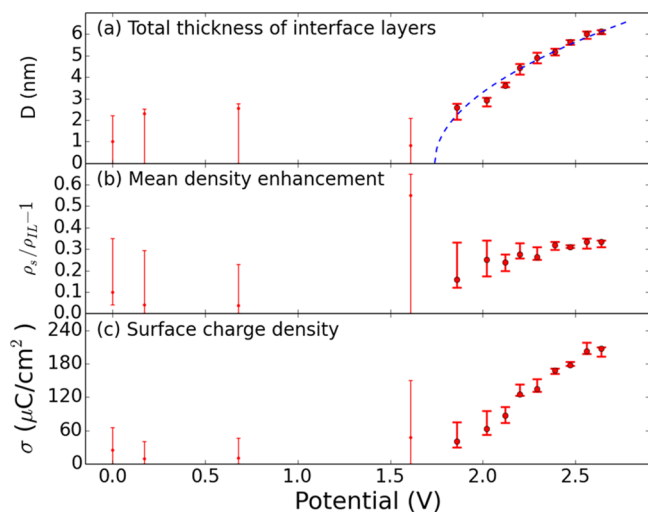


Figure 4. Best-fit parameters as a function of voltage. (a) Slab width (for one-slab fits) or total width of interface slabs (for two-slab fits). The dashed line is a fit to $D \propto \sqrt{(V - V_{\text{th}})}$ where V_{th} is a threshold voltage. (b) The interfacial slab electron density enhancement ($\rho_s - \rho_{\text{IL}})/\rho_{\text{IL}}$ where ρ_{IL} is the bulk liquid electron density (mean enhancement is shown for two-slab fits). (c) Surface charge density (anionic charge per unit area), calculated from the slab electron density assuming that the effective volumes of the cations and anions, and their charges, are fixed (these assumptions are discussed in the text).

266 if two slabs), electron density enhancement (average enhance-
267 ment if two slabs), and calculated surface charge density as
268 functions of voltage. The qualitative trends are as follows. For
269 lower voltages, when the reflectivity has no oscillatory features,
270 the error bars are large and include zero. At higher voltages the
271 interfacial density is higher than the bulk density, and this
272 means that there is an excess of anions over cations, as one
273 would expect. The average electron density varies only weakly
274 with voltage, and never reaches the density of the anion. At
275 most the interfacial layer averages $\sim 80\%$ anions, $\sim 20\%$ cations
276 (this is the number ratio; in terms of volume it is $\sim 60\%$ anions,
277 $\sim 40\%$ cations). This layer is not a monolayer; rather, above a
278 threshold voltage $V_{\text{th}} \approx 1.75$ V the slab thickness D increases
279 rapidly with voltage until it is ~ 6 nm, much larger than the
280 anion dimensions.

281 These data are consistent with the formation of a crowded
282 layer at higher voltages, as predicted^{7,13,15–18,20} but never
283 before observed, with the thickness being a strong function of
284 the applied voltage. Since the lower-voltage data show no
285 fringes, there is no significant evidence in our data of any
286 interfacial structure below the threshold voltage. Nonetheless,
287 the existence of this threshold voltage requires explanation. It is
288 likely that, for $V < V_{\text{th}}$, the interfacial electric field is balanced
289 out either by weak alternating layers of cations and anions or by
290 a diffuse Gouy–Chapman double layer as in ionic solutions.

However, these structures would have to be too weak to have
any signature in our X-ray reflectivity data.

If there is a potential difference $V - V_{\text{th}}$ across a uniform
charged slab of thickness D , Gauss’s law applied to a charged
slab requires that $D^2 = (\epsilon_0 \epsilon_r / \rho_c)(V - V_{\text{th}})$ where ρ_c is the
charge per unit volume and ϵ_r is the relative permittivity of the
material. (This equation, except for the threshold voltage V_{th} , is
equivalent to eq 23 of ref 13.) Figure 4b shows that the electron
density of the slab is at most weakly V -dependent; if we ignore
this weak dependence and assume that the slab electron density
 ρ_s and therefore the charge density ρ_c do not depend on V , we
get $D = \lambda \sqrt{(V - V_{\text{th}})}$ where $\lambda \equiv \sqrt{(\epsilon_0 \epsilon_r / \rho_c)}$ is a constant. The
dashed line in Figure 4a shows the best fit to this functional
form. Clearly the data are consistent with the predicted V
dependence. This fit gives us $V_{\text{th}} = 1.75$ V and $\lambda = 6.45$ nm
 $V^{-0.5}$.

The data in Figure 4c, which give the interfacial charge per
unit area, allow us to estimate the static (zero-frequency)
differential capacitance. Because of the scatter in the σ - V data,
it is not possible to plot the derivative $d\sigma/dV$ as a function of V
in any detail. However, we can say that, below V_{th} , the
differential capacitance due to the dense layer is indistinguish-
able from zero in our experiments, while at higher voltages the
average slope gives us ~ 200 $\mu\text{F}/\text{cm}^2$. (These numbers are in
addition to the capacitance due to any effects not observed in
our X-ray studies.)

The calculated capacitance above V_{th} is high compared to
numbers typically reported for RTILs using AC measurements
(~ 10 – 20 $\mu\text{F}/\text{cm}^2$). On the other hand, it is known³⁹ that RTIL
interfacial capacitance depends on frequency as $\omega^{-\alpha}$ where $\alpha \approx$
 0.1 – 0.3 , which (if rigorously true) would diverge in the dc
limit. This suggests that the dc capacitance of electrode–RTIL
interfaces is larger than that seen using ac measurements. The
source of such a difference would be the known low mobility of
RTIL ions. Indeed, a recent dc capacitance measurement⁴⁰ on a
different RTIL found that the differential capacitance increases
at the highest voltages studied, and reaches >50 $\mu\text{F}/\text{cm}^2$. This
increase is inconsistent with the “camel-shaped” or “bell-
shaped” curves found in ac measurements, but qualitatively
consistent with what we observe.

A second anomaly concerns the factor λ . From the electron
density data in Figure 4b: we find that the charge density ρ_c is
approximately 3×10^{-19} C/nm^3 at 2.64 V. Using this value and
the typical range of ϵ_r for bulk RTILs (~ 15 – 20),⁵ we estimate
that $\lambda \sim 0.6$ nm $V^{-0.5}$. This is an order of magnitude smaller
than the value obtained by fitting the D - V curve, and may
imply that the actual charge density is lower, the relative
permittivity is higher, or both.

Two factors not yet considered may reduce our estimates of
the surface charge density (Figure 4c). First, in the bulk RTIL,
it has been suggested that the actual ionic charges are not
integers but ~ 0.6 – 0.8 electrons/ion.^{41–44} Second, in common
with previous X-ray studies,^{24–31} our calculations above
interpreted electron density changes as due purely to anion/
cation imbalance, without considering the possibility of
compression or expansion at the interface. Lattice gas models
of RTILs¹³ assume large fractions of unoccupied sites, using a
parameter γ defined as the ratio of actual to maximum ionic
concentration (so that $1 - \gamma$ is the free volume fraction), and
suggest that γ may be as low as 0.5 even in pure RTILs.
Experimentally, however, RTILs do not appear to be very
compressible. Reference 45, using a different RTIL, reports
only a $\sim 5\%$ increase in density at 120 MPa (~ 1200 atm) 353

354 pressure. Figure 4b shows that our interfacial density increases
355 by up to 25–30% above the bulk density. It is physically
356 unreasonable to attribute any voltage-dependent density change
357 to compression alone, without attracting anions to the interface,
358 since there would then be no driving force for such
359 compression. Nonetheless our experiments cannot rule out
360 an unspecified combination of compression, fractional charges
361 per ion, and anion crowding. This would quantitatively reduce
362 but not qualitatively eliminate the charge present in the dense
363 layer (Figure 4c), and thus it would reduce the estimated
364 capacitance. Our measurements of the voltage-dependent
365 thickness of the crowded layer (Figure 4a) and our qualitative
366 conclusion that the capacitance increases across the threshold
367 voltage are, however, robust.

368 We have performed the same experiments with two other
369 RTILs (data not shown here). [TDTHP]⁺[Cl]⁻, which has the
370 same cation but a different anion, gave a null result, while
371 [N4111]⁺[NTF₂]⁻, which has the same anion but a different
372 cation, showed qualitatively similar behavior to that reported
373 above. This is reasonable: a Cl⁻ anion carries only 17 electrons
374 while [NTF₂]⁻ carries 138 electrons, so that for the same
375 amount of interfacial change, the chloride anion would create a
376 much smaller interfacial electron density enhancement. This
377 also shows that the interfacial layer must be attributed to the
378 dense [NTF₂]⁻ anion, and not to spurious effects such as
379 electrolysis products.

380 Our results provide direct confirmation of the theoretical
381 prediction that there will be a thick “crowded” layer of ions near
382 an electrode interface at higher voltages. This layer develops
383 only above a threshold voltage V_{th} . Unexpectedly, the crowded
384 layer is not purely anionic, but at most ~80% anions and 20%
385 cations. We see no evidence of either alternating layers of
386 anions and cations (“overcharging”) or a diffuse layer in our
387 system, although it is likely that there are interfacial structures
388 below our level of detection. Further, our data imply that the
389 DC differential capacitance is larger at higher voltages, and the
390 permittivity of the interfacial layer may also be large. Both these
391 possibilities have significant implications for the use of RTILs
392 for energy storage and in electrochemical devices, and illustrate
393 the complexity and novelty of this class of liquid electrolytes.

394 ■ METHODS

395 Trihexyltetradecylphosphonium bis(trifluoromethylsulfonyl)-
396 imide ([TDTHP]⁺[NTF₂]⁻) was purchased from Stem
397 Chemicals. Figure 1 shows the anion and cation. The RTIL
398 was placed in a vacuum oven for 24 h to remove water at 373
399 K. P-type (111) silicon chips (5 mm × 7 mm) were purchased
400 from Ted-Pella. To obtain an atomistic flat surface,⁴⁶ we used a
401 rapid thermal process (AW-610) in oxygen to grow a layer of
402 thermal oxide of ~400 Å on the silicon surfaces. This layer was
403 removed with buffered oxide etch, exposing ultraflat fresh
404 silicon (111) surfaces. The silicon chip was mounted to a
405 transmission cell (made of Kel-F, with Kapton windows) and
406 connected as the working electrode. Gold wires were used to
407 electrically connect to the chip, and also used as counter and
408 pseudoreference electrodes within the liquid. Although a thin
409 liquid film sample cell^{30,47} causes less attenuation of X-rays
410 traveling through the RTIL, we did not use such a setup
411 because of the high resistivity of RTILs and the resulting risk of
412 nonuniform interfacial potential. The external voltage was
413 controlled with a potentiostat (DY2311, Ivy-Digital).

414 Figure 1 shows the layout of the experiment. The specular
415 reflectivity was measured in the transmission geometry as a

function of wave transfer, $k = 2\pi \sin \theta/\lambda$. The thickness of the
416 transmission cell in the direction of the X-ray beam was 6 mm,
417 and the width of the silicon substrate in the beam direction was
418 5 mm. The experiment was conducted at Sectors 12BM-B and
419 33BM-C of the Advanced Photon Source, with X-ray energy of
420 19.3 keV. An area detector Pilatus 100 K was used to
421 simultaneously record the specular reflectivity signal as well as
422 the off-specular background (± 0.2 degree off the specular beam
423 in the χ direction). 424

■ ASSOCIATED CONTENT

Supporting Information

The Supporting Information is available free of charge on the
427 ACS Publications website at DOI: 10.1021/acscentsci.6b00014. 428

Best-fit parameters, comparison of one- and two-slab
429 model fits, electron density data, rationale for choice of Si
430 electrode, and results of attempted fitting using the
431 distorted crystal model (PDF) 432

■ AUTHOR INFORMATION

Corresponding Author

*E-mail: pputta@northwestern.edu. 435

Notes

The authors declare no competing financial interest. 437

■ ACKNOWLEDGMENTS

This research was supported by the U.S. National Science
439 Foundation under Grant No. DMR-1309589. This work
440 utilized Northwestern University’s Micro/Nano Fabrication
441 Facility (NUFAB), which is supported by the State of Illinois
442 and Northwestern University. The X-ray reflectivity measure-
443 ments were performed at Beamlines 12BM-B and 33BM-C of
444 the Advanced Photon Source, which are supported by the U.S.
445 Department of Energy under Contract No. DE-AC02-
446 06CH11357. The authors thank Sungsik Lee, Benjamin
447 Reinhart, and Jenia Karapetrova for their assistance during
448 the experiments, and Ahmet Uysal for valuable discussions. 449

■ REFERENCES

- (1) Hayes, R.; Warr, G. G.; Atkin, R. Structure and nanostructure in
451 ionic liquids. *Chem. Rev.* **2015**, *115*, 6357–6426. 452
- (2) Rogers, R. D.; Seddon, K. R. Ionic liquids—solvents of the future?
453 *Science* **2003**, *302*, 792–793. 454
- (3) Welton, T. Room-Temperature Ionic Liquids. Solvents for
455 Synthesis and Catalysis. *Chem. Rev.* **1999**, *99*, 2071–2083. 456
- (4) Simon, P.; Gogotsi, Y. Materials for electrochemical capacitors.
457 *Nat. Mater.* **2008**, *7*, 845–854. 458
- (5) Fedorov, M. V.; Kornyshev, A. A. Ionic liquids at electrified
459 interfaces. *Chem. Rev.* **2014**, *114*, 2978–3036. 460
- (6) Abbott, A. P.; Frisch, G.; Ryder, K. S. Electroplating Using Ionic
461 Liquids. *Annu. Rev. Mater. Res.* **2013**, *43*, 335–358. 462
- (7) Fedorov, M. V.; Kornyshev, A. A. Towards understanding the
463 structure and capacitance of electrical double layer in ionic liquids.
464 *Electrochim. Acta* **2008**, *53*, 6835–6840. 465
- (8) Gebbie, M. A.; Valtiner, M.; Banquy, X.; Henderson, W. A.;
466 Israelachvili, J. N. Reply to Perkin et al.: Experimental observations
467 demonstrate that ionic liquids form both bound (Stern) and diffuse
468 electric double layers. *Proc. Natl. Acad. Sci. U. S. A.* **2013**, *110*, E4122–
469 E4122. 470
- (9) Gebbie, M. A.; Valtiner, M.; Banquy, X.; Fox, E. T.; Henderson,
471 W. A.; Israelachvili, J. N. Ionic liquids behave as dilute electrolyte
472 solutions. *Proc. Natl. Acad. Sci. U. S. A.* **2013**, *110*, 9674–9679. 473

- 474 (10) Perkin, S.; Salanne, M.; Madden, P.; Lynden-Bell, R. Is a Stern
475 and diffuse layer model appropriate to ionic liquids at surfaces? *Proc.*
476 *Natl. Acad. Sci. U. S. A.* **2013**, *110*, E4121.
- 477 (11) Schmickler, W.; Santos, E. *Interfacial electrochemistry*; Springer-
478 Verlag: Berlin, 2010; pp 1–272.
- 479 (12) Bedzyk, M. J.; Bommarito, G. M.; Caffrey, M.; Penner, T. L.
480 Diffuse-double layer at a membrane-aqueous interface measured with
481 x-ray standing waves. *Science* **1990**, *248*, 52–56.
- 482 (13) Kornyshev, A. A. Double-layer in ionic liquids: Paradigm
483 change? *J. Phys. Chem. B* **2007**, *111*, 5545–5557.
- 484 (14) Kirchner, K.; Kirchner, T.; Ivaniššev, V.; Fedorov, M. V.
485 Electrical double layer in ionic liquids: Structural transitions from
486 multilayer to monolayer structure at the interface. *Electrochim. Acta*
487 **2013**, *110*, 762–771.
- 488 (15) Fedorov, M. V.; Kornyshev, A. A. Ionic liquid near a charged
489 wall: Structure and capacitance of electrical double layer. *J. Phys. Chem.*
490 *B* **2008**, *112*, 11868–11872.
- 491 (16) Fedorov, M. V.; Kornyshev, A. A. Erratum: Ionic Liquid Near a
492 Charged Wall: Structure and Capacitance of Electrical Double Layer. *J.*
493 *Phys. Chem. B* **2009**, *113*, 4500.
- 494 (17) Bazant, M. Z.; Storey, B. D.; Kornyshev, A. A. Double Layer in
495 Ionic Liquids: Overscreening versus Crowding. *Phys. Rev. Lett.* **2011**,
496 *106*, 046102.
- 497 (18) Bazant, M.; Storey, B.; Kornyshev, A. Erratum: Double Layer in
498 Ionic Liquids: Overscreening versus Crowding [Phys. Rev. Lett. 106,
499 046102 (2011)]. *Phys. Rev. Lett.* **2012**, *109*, 149903.
- 500 (19) Ivanistsev, V.; Fedorov, M. V.; Lynden-Bell, R. M. Screening of
501 Ion-Graphene Electrode Interactions by Ionic Liquids: The Effects of
502 Liquid Structure. *J. Phys. Chem. C* **2014**, *118*, 5841–5847.
- 503 (20) Ivaniššev, V.; Fedorov, M. Interfaces between Charged Surfaces
504 and Ionic Liquids: Insights from Molecular Simulations. *Electrochem.*
505 *Soc. Interface* **2014**, *23*, 65–69.
- 506 (21) Kornyshev, A. A.; Qiao, R. Three-dimensional double layers. *J.*
507 *Phys. Chem. C* **2014**, *118*, 18285–18290.
- 508 (22) Bowers, J.; Vergara-Gutierrez, M. C.; Webster, J. R. P. Surface
509 Ordering of Amphiphilic Ionic Liquids. *Langmuir* **2004**, *20*, 309–312.
- 510 (23) Lauw, Y.; Horne, M. D.; Rodopoulos, T.; Lockett, V.; Akgun, B.;
511 Hamilton, W. A.; Nelson, A. R. J. Structure of [C 4 mpyr][NTf 2]
512 Room-Temperature Ionic Liquid at Charged Gold Interfaces.
513 *Langmuir* **2012**, *28*, 7374–7381.
- 514 (24) Mezger, M.; Schröder, H.; Reichert, H.; Schramm, S.; Okasinski,
515 J. S.; Schöder, S.; Honkimäki, V.; Deutsch, M.; Ocko, B. M.; Ralston,
516 J.; Rohwerder, M.; Stratmann, M.; Dosch, H. Molecular layering of
517 fluorinated ionic liquids at a charged sapphire (0001) surface. *Science*
518 **2008**, *322*, 424–428.
- 519 (25) Mezger, M.; Schramm, S.; Schröder, H.; Reichert, H.; Deutsch,
520 M.; De Souza, E. J.; Okasinski, J. S.; Ocko, B. M.; Honkimäki, V.;
521 Dosch, H. Layering of [BMIM]⁺-based ionic liquids at a charged
522 sapphire interface. *J. Chem. Phys.* **2009**, *131*, 094701.
- 523 (26) Brkljača, Z.; Klimczak, M.; Miličević, Z.; Weisser, M.; Taccardi,
524 N.; Wasserscheid, P.; Smith, D. M.; Magerl, A.; Smith, A.-S. a.
525 Complementary Molecular Dynamics and X-ray Reflectivity Study of
526 an Imidazolium-Based Ionic Liquid at a Neutral Sapphire Interface. *J.*
527 *Phys. Chem. Lett.* **2015**, *6*, 549–555.
- 528 (27) Zhou, H.; Rouha, M.; Feng, G.; Lee, S. S.; Docherty, H.; Fenter,
529 P.; Cummings, P. T.; Fulvio, P. F.; Dai, S.; McDonough, J.; Presser, V.;
530 Gogotsi, Y. Nanoscale perturbations of room temperature ionic liquid
531 structure at charged and uncharged interfaces. *ACS Nano* **2012**, *6*,
532 9818–9827.
- 533 (28) Uysal, A.; Zhou, H.; Feng, G.; Lee, S. S.; Li, S.; Cummings, P.
534 T.; Fulvio, P. F.; Dai, S.; McDonough, J. K.; Gogotsi, Y. Interfacial
535 ionic 'liquids': connecting static and dynamic structures. *J. Phys.:*
536 *Condens. Matter* **2015**, *27*, 032101.
- 537 (29) Yu, C.-J.; Richter, A.; Datta, A.; Durbin, M.; Dutta, P.
538 Observation of molecular layering in thin liquid films using X-ray
539 reflectivity. *Phys. Rev. Lett.* **1999**, *82*, 2326.
- 540 (30) Yamamoto, R.; Morisaki, H.; Sakata, O.; Shimotani, H.; Yuan,
541 H.; Iwasa, Y.; Kimura, T.; Wakabayashi, Y. External electric field
dependence of the structure of the electric double layer at an ionic
liquid/Au interface. *Appl. Phys. Lett.* **2012**, *101*, 053122.
- (31) Uysal, A.; Zhou, H.; Feng, G.; Lee, S. Structural Origins of
Potential Dependent Hysteresis at the Electrified Graphene/Ionic
Liquid Interface. *J. Phys. Chem. C* **2014**, *118*, 569–574.
- (32) Hayes, R.; Borisenko, N.; Tam, M. K.; Howlett, P. C.; Endres,
F.; Atkin, R. Double Layer Structure of Ionic Liquids at the Au(111)
Electrode Interface: An Atomic Force Microscopy Investigation. *J.*
Phys. Chem. C **2011**, *115*, 6855–6863.
- (33) Black, J. M.; Walters, D.; Labuda, A.; Feng, G.; Hillesheim, P.
C.; Dai, S.; Cummings, P. T.; Kalinin, S. V.; Proksch, R.; Balke, N.
Bias-Dependent Molecular-Level Structure of Electrical Double Layer
in Ionic Liquid on Graphite. *Nano Lett.* **2013**, *13*, 5954–5960.
- (34) Hayyan, M.; Mjalli, F. S.; Hashim, M. A.; AlNashef, I. M.; Mei,
T. X. Investigating the electrochemical windows of ionic liquids. *J. Ind.*
Eng. Chem. **2013**, *19*, 106–112.
- (35) Zhang, S.; Sun, N.; He, X.; Lu, X.; Zhang, X. Physical properties
of ionic liquids: Database and evaluation. *J. Phys. Chem. Ref. Data*
2006, *35*, 1475–1517.
- (36) Binnig, G.; Rohrer, H.; Gerber, C.; Weibel, E. 7 × 7
reconstruction on Si (111) resolved in real space. *Phys. Rev. Lett.*
1983, *50*, 120.
- (37) Sloutskin, E.; Ocko, B. M.; Tamam, L.; Kuzmenko, I.; Gog, T.;
Deutsch, M. Surface Layering in Ionic Liquids: An X-ray Reflectivity
Study. *J. Am. Chem. Soc.* **2005**, *127*, 7796–7804.
- (38) Kilic, M. S.; Bazant, M. Z.; Ajdari, A. Steric effects in the
dynamics of electrolytes at large applied voltages. I. Double-layer
charging. *Phys. Rev. E* **2007**, *75*, 1–16.
- (39) Lockett, V.; Sedev, R.; Ralston, J.; Horne, M.; Rodopoulos, T.
Differential Capacitance of the Electrical Double Layer in
Imidazolium-Based Ionic Liquids: Influence of Potential, Cation
Size, and Temperature. *J. Phys. Chem. C* **2008**, *112*, 7486–7495.
- (40) Nishi, N.; Hashimoto, A.; Minami, E.; Sakka, T. Electro-
capillarity and zero-frequency differential capacitance at the interface
between mercury and ionic liquids measured using the pendant drop
method. *Phys. Chem. Phys.* **2015**, *17*, 5219–5226.
- (41) Schmidt, J.; Krekeler, C.; Dommert, F.; Zhao, Y.; Berger, R.;
Site, L. D.; Holm, C. Ionic charge reduction and atomic partial charges
from first-principles calculations of 1,3-dimethylimidazolium chloride.
J. Phys. Chem. B **2010**, *114*, 6150–6155.
- (42) Hollóczy, O.; Malberg, F.; Welton, T.; Kirchner, B. On the
origin of ionicity in ionic liquids. Ion pairing versus charge transfer.
Phys. Chem. Chem. Phys. **2014**, *16*, 16880–16890.
- (43) Del Pópolo, M. G.; Lynden-Bell, R. M.; Kohanoff, J. Ab initio
molecular dynamics simulation of a room temperature ionic liquid. *J.*
Phys. Chem. B **2005**, *109*, 5895–5902.
- (44) Youngs, T. G.; Hardacre, C. Application of static charge transfer
within an ionic-liquid force field and its effect on structure and
dynamics. *ChemPhysChem* **2008**, *9*, 1548–1558.
- (45) Gacino, F. M.; Regueira, T.; Comunas, M. J. P.; Lugo, L.;
Fernandez, J. Density and isothermal compressibility for two
trialkylimidazolium-based ionic liquids at temperatures from (278 to
398) K and up to 120 MPa. *J. Chem. Thermodyn.* **2015**, *81*, 124–130.
- (46) Higashi, G. S.; Chabal, Y. J.; Trucks, G. W.; Raghavachari, K.
Ideal hydrogen termination of the Si (111) surface. *Appl. Phys. Lett.*
1990, *56*, 656–658.
- (47) Fenter, P.; Sturchio, N. C. Mineral–water interfacial structures
revealed by synchrotron X-ray scattering. *Prog. Surf. Sci.* **2004**, *77*,
171–258.